Investigating the Photoluminescent Properties of Fe^{3+} doped $ZnAl_2O_4$: A Multifunctional Material for Emerging Applications.

E.D. Magasi.[1], O.M. Ntwaeaborwa[2], M.L.A. Letswalo[1], B.M. Sondezi[1]

[1]Physics Department, University of Johannesburg, Auckland Park, Johannesburg 2006, South Africa.
[2]Department of Physical and Earth science, Sol Plaatjie University, Kimberley 8301, South Africa.

E-mail: bmsondezi@uj.ac.za and letswalom@uj.ac.za

Abstract. Zinc aluminate ($ZnAl_2O_4$) is a member of the spinel family which has attracted great research interest due to its diverse properties such as hydrophobicity, chemical stability, impressive fluorescence efficiency, and thermal stability. These properties make it a suitable candidate for application in displays, magnetic refrigerators, catalysis, and light emitting diodes (LED). In this study, a well separated $ZnAl_2O_4$ doped with Fe^{3+} ions was synthesised via Pechini synthesis method. XRD spectra confirmed the formation of a pure $ZnAl_2O_4$ material that crystallized in single-phase cubic symmetry belonging to the Fd3m space group of $ZnAl_2O_4$. This crystal structure was not affected by the incorporation of Fe^{3+} ions, indicating a successful substitution of Fe^{3+} ions into the $ZnAl_2O_4$ lattice sites. Energy dispersive spectroscopy was used for elemental composition investigations which validated Zn, Al, and O's presence in pristine sample and confirmed the presence of Zn, Al, O, and Fe in doped $ZnAl_2O_4$ samples. Photoluminescence (PL) spectroscopy, excited using a xenon lamp, revealed two broad emission bands at approximately 440 nm and 745 nm. These emissions are attributed to the $^4T_1 \rightarrow {}^6A_1$ and $^4T_2 \rightarrow {}^6A_1$ transitions of Fe^{3+} ions, which occupy the tetrahedral (Tet) and the octahedral (Oct) coordination sites, respectively, within the $ZnAl_2O_4$ lattice. The CIE (Commission Internationale de I'Eclairage) confirmed that pure $ZnAl_2O_4$ color emission was lying in the blue region and upon doping with varying concentrations of Fe^{3+}, the coordinates were tuned towards the white colour region, indicating a potential for tunable white emission.

1 Introduction

Zinc aluminate ($ZnAl_2O_4$) is a significant member of the spinel-aluminate group which has gained enormous scientific attention in the last three decades due to their outstanding physical and chemical properties [1,2]. These unique sets of properties facilitate their extensive use in applications such ceramics [3], displays [4], and light emitting diodes [5]. Additionally, its wide direct band gap of 3.8 eV enables its utilization as a dielectric material, sensor, and optical material [6]. This wide bandgap can be tuned by introducing rare earth or transition metals as dopants to serve as luminescent centers. The emergence of several reports on $ZnAl_2O_4$ doped with transition metals and rare earth ions shows that there is a clear consensus in the scientific community that $ZnAl_2O_4$ is a promising host material for several activator ions [7, 8]. The intended application informs the researcher about the appropriate dopant and dopant concentration required. For economic reasons, doping with transition metals is explored by researchers in addition to doping with rare earth ions. Additionally, $ZnAl_2O_4$ doped with transition metals have gained attention because of the interesting luminescent properties which are induced by the unique electron configuration of these transition metals. Moreover, transition metals are suitable for tunable radiation sources in optical devices because of their unique emission observed in both the visible and infrared regions [9]. Fe^{3+} in particular, has broadband emissions in the higher energy region when doped in tetrahedral site and in the lower energy region when doped in octahedral site [9].

Literature shows that several researchers do not consider the effects of charge imbalance when doping and this can lead to poor luminescence efficiency via the formation of charge defects [10-12]. Therefore, this study investigates how Fe^{3+} incorporation into the Al^{3+} site of $ZnAl_2O_4$ affects the crystal structure and

photoluminescence characteristics while maintaining charge balance, with a view toward optimizing white-light emission for LED applications. Charge balance was maintained by substituting a trivalent ion (Al^{3+}) with another trivalent ion (Fe^{3+}) ensuring a direct charge balanced system.

2 Experimental details

2.1 Sample preparation

Pechini synthesis was used to prepare $ZnAl_2O_4$ phosphors doped with varying mol% of Fe^{3+}. The starting materials included zinc nitrate hexahydrate ($Zn(NO_3)_2{\cdot}6H_2O$) (99.98%), aluminum nitrate nonahydrate ($Al(NO_3)_3{\cdot}9H_2O$) (99.98%), iron nitrate nonahydrate ($Fe(NO_3)_3{\cdot}9H_2O$) (>98%), tartaric acid ($C_4H_6O_6$) and nitric acid (HNO_3). The pristine sample was prepared by dissolving stoichiometric amounts of $Zn(NO_3)_2{\cdot}6H_2O$ and $Al(NO_3)_3{\cdot}9H_2O$ in 10 millilitres of nitric acid in a glass beaker, and $C_4H_6O_6$ in 40 millilitres of distilled water in a separate glass beaker. Separately, the two solutions were stirred for 20 minutes at 150 ℃ on a hot plate. The two solutions were then mixed, and the mixture was stirred at 150 ℃ for about 2 hours forming a polymerized resin. After 10 hours of drying at 80 ℃, the sample was crushed into a fine powder and calcined for 3 hours at 600 ℃. The same procedure was repeated with stoichiometric amount of $Fe(NO_3)_3{\cdot}9H_2O$ added to substitute $Al(NO_3)_3{\cdot}9H_2O$ for the synthesis of $ZnAl_{(2-x)}Fe_xO_4$ (x = 0.01, 0.025, 0.05, 0.08 mol%) samples.

2.2 Instrumentation

Powder X-ray diffraction (XRD) investigation using Cu K_α ($\lambda = 1.5405$Å) radiation on a MiniFlex600 diffractometer at 40 kV and 15 mA was conducted to characterize the crystal structures. A scanning electron microscope (SEM, TESCAN VEGA 3 XMU, LMH instrument, Brno, Czech Republic) in conjunction with energy dispersive X-ray spectroscopy (EDS) was used to analyse the particle morphology of the sample. A Horiba QM8000 spectrofluorometer equipped with double excitation and emission monochromators was used to measure photoluminescence spectra. The signal from the sample was detected using a PPD-850 Si photodiode detector, and the excitation source was a Xe lamp.

3 Results and Discussion

3.1 Powder X-ray diffraction analysis

The X-ray diffraction (XRD) patterns of $ZnAl_{(2-x)}Fe_xO_4$ (x=0, 0.01, 0.025, 0.05, 0.08 mol%) are shown in fig. 1(a). The peaks of all the synthesized samples are consistent with the standard phase data of $ZnAl_2O_4$ referenced from JCPDS file no. 82-1043. The absence of impurity or additional peaks from these samples indicates a single-phase formation suggesting that the materials crystallized in a single-phase cubic spinel compound belonging to $Fd3m$ space group of $ZnAl_2O_4$. The phase structure of $ZnAl_2O_4$ phosphors was not altered when the Fe^{3+} ions concentration was increased and this shows that $ZnAl_{(2-x)}Fe_xO_4$ powder samples were successfully synthesized.

Samples	Lattice parameters
	a (Å)
X = 0	8.089
X = 0.01	8.081
X = 0.025	8.087
X = 0.05	8.082
X = 0.08	8.091

Table 1: Depicts estimated lattice parameters of $ZnAl_{(2-x)}Fe_xO_4$ (x=0, 0.01, 0.025, 0.05, 0.08 mol%).

It is apparent from Fig. 1(a) that peak (311) is the most intense and was subsequently used to analyze the effects of doping on the peak position as shown in Fig. 1(b). A noticeable shift towards smaller angles was

observed and this reveals that the dimension of unit cell (cell parameter) is affected by doping with Fe^{3+} ions as depicted in table 1. This change of lattice parameters may be attributed to the substitution of an ion with a smaller ionic radius (Al^{3+} =0.054 nm) by an ion with a larger ionic radius (Fe^{3+}=0.065 nm). Similar results have been reported by several researchers when substituting ions of different ionic radius [13, 14].

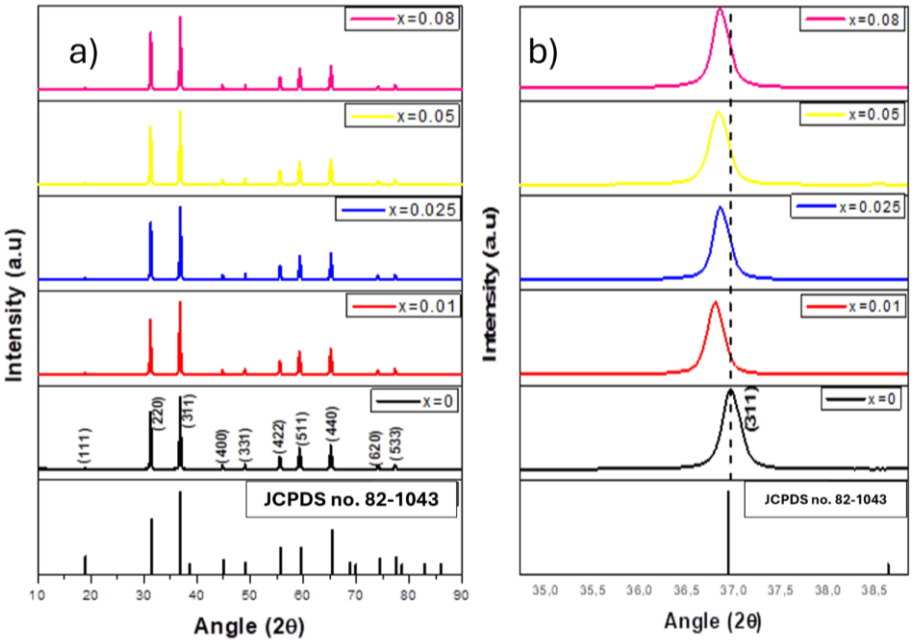

Figure 1: (a) XRD pattern of $ZnAl_{(2-x)}Fe_xO_4$(x=0, 0.01, 0.025, 0.05, and 0.08 mol%) and (b) enlarged XRD pattern of high intensity (311).

3.2 Morphological and chemical composition analysis

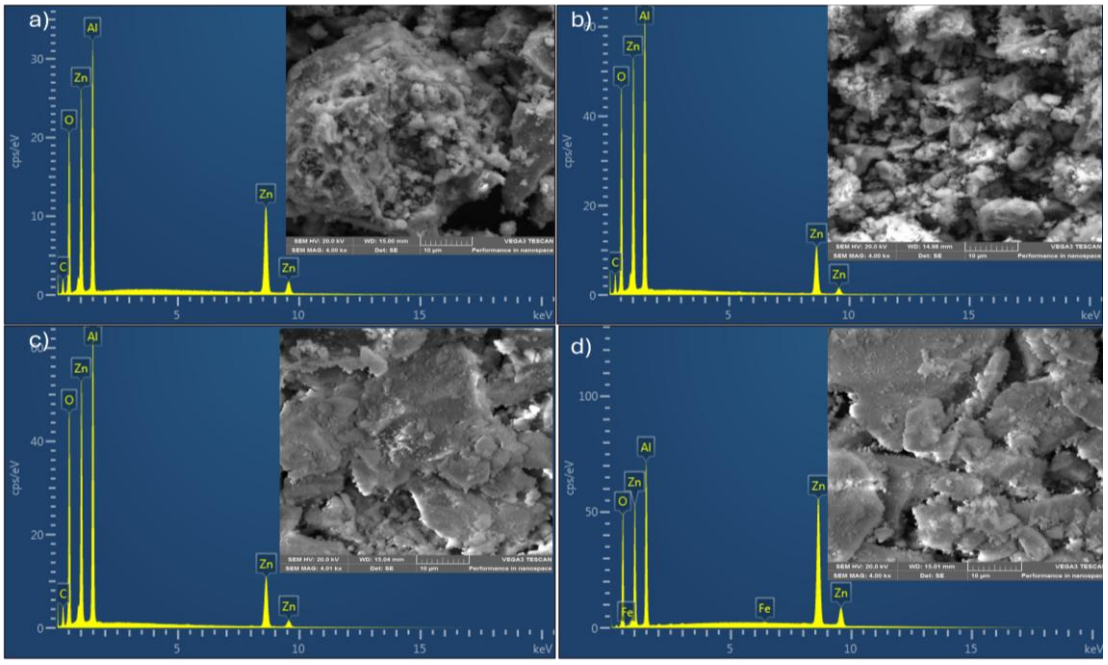

Figure 2: EDS spectrum and SEM images of $ZnAl_{(2-x)}Fe_xO_4$ (a) x = 0, (b) x = 0.01, x = 0.05 and (c) x = 0.08.

The morphology of the $ZnAl_{(2-X)}Fe_xO_4$ phosphor materials were examined from the SEM images as shown in Fig 2. Fig 2(a) depicts the morphology of the pristine $ZnAl_2O_4$ which is characterized by irregular shaped particles with small particles encrusted on the surface of larger particles. These irregular shaped particles are reduced in size upon doping with 0.01 mol% of Fe^{3+} as shown in Fig. 2(b). Further increment of the dopant concentration to 0.05 and 0.08 mol% resulted in the morphology of the samples showing soft agglomerates that display plate-like irregular morphology with observable grain boundaries and small particles encrusted on the surface of larger particles as seen in Fig. 2(c and d). The presence of Zn, Al, and O in the pristine sample and Fe in the 0.08 mol% doped sample are confirmed by the EDS spectra displayed in Fig 2(a) and Fig 2(d), respectively. Fe ions were not detected for 0.05 mol% doped sample in Fig. 2(c), and this is probably due to lower dopant concentration which may be below the detection limit of the instrument. The carbon that is detected in these samples is from the carbon coating used to coat samples and does not come from the samples.

3.3 Photoluminescence studies

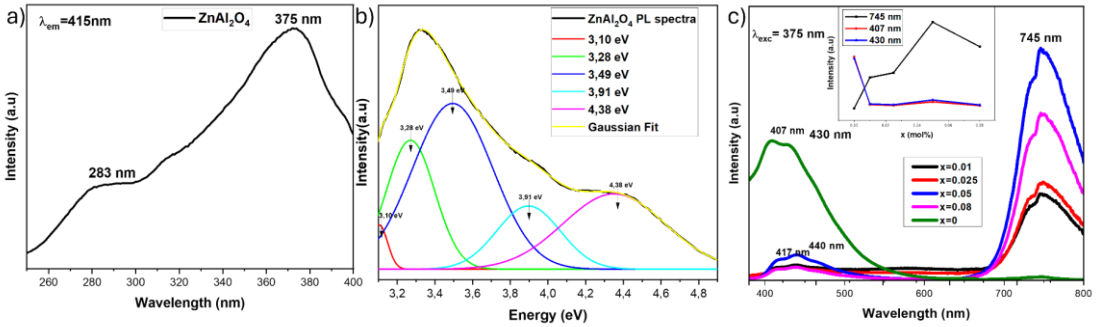

Figure 7: The PL (a) excitation (under λ_{em}= 415 nm) spectra of $ZnAl_2O_4$, (b) the deconvoluted PL excitation spectra of $ZnAl_2O_4$ and (c) emission spectra (under λ_{ex}=375 nm) of $ZnAl_{(2-x)}Fe_xO_4$(x=0, 0.01, 0.025, 0.05, and 0.08 mol%) phosphors. The variation of 407, 430, and 745 nm peaks as a function of Fe^{3+} concentration is shown in the inset of (c).

The PL excitation spectra of $ZnAl_2O_4$ phosphors was obtained while maintaining the emission wavelength at 415 nm and scanning the spectrum in the wavelength range of 250-400 nm as displayed in Fig. 3(a). In the excitation spectra, two prominent broad bands with peaks at 283 and 375 nm were observed and are attributable to the band-to-band transition of $ZnAl_2O_4$ [7,15]. The deconvoluted excitation PL spectra of the undoped $ZnAl_2O_4$ shown in Fig. 3(b), exhibits a broad band between 3 and 4.8 eV. The most prominent broad peak which has a maximum at 3.49 eV is assigned to the band-to-band transition of the AlO_6 anion grouping of $ZnAl_2O_4$, while the 3.28 eV peak is due to the intrinsic intra-bandgap defects such as oxygen vacancies (V_o) of $ZnAl_2O_4$ [9,16]. There is limited literature reporting the 3.10 and 3.91 eV peaks.

The PL emission spectra of the $ZnAl_{(2-x)}Fe_xO_4$ (x = 0, 0.01, 0.025, 0.05, and 0.08 mol%) are shown in Fig. 3(c). 407, 430 and 745 nm peaks are observed in this emission spectra with the 407 and 430 nm peaks red shifted to 417 and 440 nm, respectively, upon the introduction of Fe^{3+} dopant into the host material. Doping with Fe^{3+} ions clearly quenches the emission intensities of the 407 and 430 nm peaks and improves the intensity of the 745 nm peak, as can be seen in the emission spectra. The maximum intensities of the 407 and 430 nm peaks are observed in pristine $ZnAl_2O_4$ and their quenching upon doping with Fe^{3+} suggests that these peaks can be attributed to the defect related intra-band transitions such as oxygen vacancies (V_o) and Zn^{2+} interstitials in the spinel lattice which are reduced by the introduction of Fe^{3+} ions [5,17]. Several researchers have observed similar cationic redistribution effects and the quenching of the defect related emissions when introducing Fe^{3+} ions into the crystal structures of different host materials such as ZnO and ZnS with Fe^{3+} [18,19]. This further suggests that the radiative transitions changed and $ZnAl_2O_4$ no longer emits but rather captures primary excited energy and transfers it to Fe^{3+} dopants. The relation between emission intensities and Fe^{3+} concentration is depicted in the insert of Fig. 3(c). This inset shows a sharp drop of the 407 and 430 nm peaks and an enhancement of the 745 nm peak upon the introduction of Fe^{3+} dopant.

The intensity of the 745 nm peak on the other hand increased remarkably upon doping with Fe^{3+} ions with the maximum intensity observed when x = 0.05 mol% Fe^{3+} doping concentration beyond which the emission intensity decreases. This quenching of the emission intensity at higher concentration can be attributed to concentration quenching effects. The 417 and 440 nm emission peaks can be attributed to tetrahedral coordinated Fe^{3+} ions while the 745 nm peak can be attributed to the octahedral coordinated Fe^{3+} ions because $ZnAl_2O_4$ has two different substitutional sites namely, tetrahedral, and octahedral site and Fe^{3+} dopants emit at shorter wavelength (blue region) when occupying tetrahedral sites and emit at longer wavelength (red region) when occupying octahedral site [7]. Pathak et al. [8] observed similar peaks at 440 and 740 nm which were attributed to the tetrahedral coordinated and octahedral coordinated Fe^{3+} ions respectively. Furthermore, the emission from the tetrahedral coordinated Fe^{3+} ions in this study is ascribed to the $^4E + {}^4A_1(^4G) \rightarrow {}^6A_1(^6S)$ transition, while the emission related to the octahedral coordinated Fe^{3+} ions belongs to the $^4T_2(^4G) \rightarrow {}^6A_1(^6S)$ transition [20, 21].

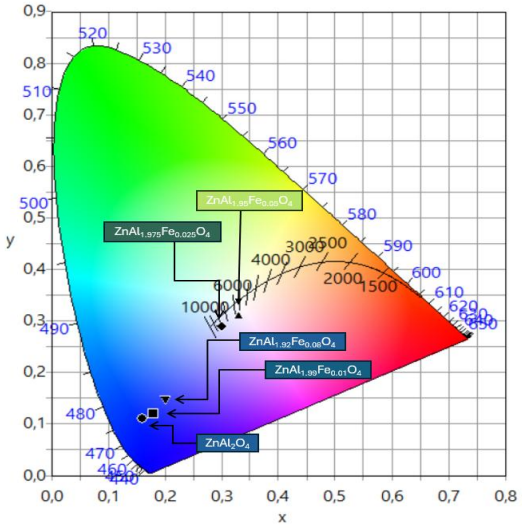

Figure 8: CIE chromaticity diagram of $ZnAl_{(2-x)}Fe_xO_4$ (x=0, 0.01, 0.025, 0.05, and 0.08 mol%).

From the emission spectra, the CIE coordinates of $ZnAl_{(2-x)}Fe_xO_4$ phosphors were calculated to determine the possible color emission points lying on the horse-shoe curve of the visible spectrum as shown in Fig. 8. The calculated color coordinates (x, y) of pure $ZnAl_2O_4$ were found to be (0.16; 0.11) which shifted towards the white region upon doping with Fe^{3+}. Doping with x = 0.05 mol% Fe^{3+} ions influenced these coordinates and shifted them to (0.33; 0.31), which are closer to those of white color coordinates. The standard coordinates of white color are (0.33; 0.33) [5]. Increasing the Fe^{3+} dopants concentration to x = 0.08 shifted the coordinates to (0.30; 0.29), which is a shift towards the blue region. This indicates that $ZnAl_{(2-x)}Fe_xO_4$ is a promising phosphor for use as sources of blue and white light in LED lighting systems.

4 Conclusion

In this work, the effects of Fe^{3+} concentration on the photoluminescent properties of $ZnAl_2O_4$ were investigated. The XRD patterns demonstrated a successful crystallization of a single-phase $ZnAl_2O_4$ that was not affected by the Fe^{3+} doping. PL emission peaks attributable to defect related intra-band transitions were observed for undoped $ZnAl_2O_4$ and were quenched upon doping with Fe^{3+}. Significant enhancement of the 745 nm peak attributed to octahedrally coordinated Fe^{3+} was observed with the maximum emission peak observed for 0.05 mol% doped sample above which the intensity dropped. Pristine $ZnAl_2O_4$ emitted in the blue region which shifted towards white color upon doping. These findings not only contribute to understanding transition metal-doped spinel phosphors but also pave the way for designing efficient, tunable phosphor materials for LED technology.

5 References

1. Xu, Z., Li, Y., Liu, Z. and Xiong, Z., 2004. Low-temperature synthesis of nanocrystalline $ZnGa_2O_4$: Tb^{3+}phosphors via the Pechini method. Materials Science and Engineering: B, 110(3), pp.302-306.
2. Lahmer, M.A., 2019. The effect of Fe^{3+}-doping on the electronic, optical and magnetic properties of $ZnAl_2O_4$; a first-principles study. Computational Condensed Matter, 20(14), pp.387-392.
3. Duan, X., Yuan, D., Wang, X. and Xu, H., 2005. Synthesis and characterization of nanocrystalline zinc aluminium spinel by a new sol-gel method. Journal of sol-gel science and technology, 35(3), pp.221-224.
4. Huang, B., Chang, Y.S., Chen, H.L., Hwang, C.C., Jian, C.J., Chen, Y.S. and Tsai, M.T., 2014. Preparation and luminescence of green-emitting $ZnAl_2O_4$:Mn^{2+} phosphor thin films. Thin Solid Films, 570(9), pp.451-456.
5. Zhang, D., Zhu, B., Ren, S., Wang, Q., Wang, Q., Li, S., Zhang, B. and Wang, W., 2021. The white light caused by defects and complex cation distribution in $ZnAl_{(2-x)}Fe_xO_4$ magnetic nanocrystals. Materials Research Express, 8(12), pp.2590-2601.
6. ameera, S., Vidyadharan, V., Sasidharan, S. and Gopchandran, K.G., 2019. Nanostructured zinc aluminates: A promising material for cool roof coating. Journal of Science: Advanced Materials and Devices, 4(4), pp.524-530.
7. Ogugua, S.N., Ntwaeaborwa, O.M. and Swart, H.C., 2021. Luminescence, structure, and insight on the inversion degree from normal to inverse spinel in a $ZnAl_{(2-x)}Fe^{3+}{}_XO_4$ system. Boletín de la Sociedad Española de Cerámica y Vidrio, 60(3), pp.147-162.
8. Pathak, N., Gupta, S.K., Sanyal, K., Kumar, M., Kadam, R.M. and Natarajan, V., 2014. Photoluminescence and EPR studies on Fe^{3+} doped $ZnAl_2O_4$: an evidence for local site swapping of Fe^{3+} and formation of inverse and normal phase. Dalton Transactions, 43(24), pp.9313-9323.
9. Ravikumar, B.S., Nagabhushana, H., Sharma, S.C. and Nagabhushana, B.M., 2014. Low temperature synthesis, structural and dosimetric characterization of $ZnAl_2O_4$: Ce^{3+}nanophosphor. *Spectrochimica Acta Part A: Molecular and Biomolecular Spectroscopy, 122*(6), pp.489-498.
10. Kumari, P. and Dwivedi, Y., 2016. Structural and photophysical investigations of bright yellow emitting Dy:$ZnAl_2O_4$ nanophosphor. Journal of Luminescence, 178(3), pp.407-413
11. Bouguerra, M., Samah, M., Belkhir, M.A., Chergui, A., Gerbous, L., Nouet, G., Chateigner, D. and Madelon, R., 2006. Intense photoluminescence of slightly doped ZnO–SiO_2 matrix. Chemical physics letters, 425(1-3), pp.77-81.
12. Jain, M., Manju, Kumar, M., Lee, H.H., Won, S.O., Chae, K.H., Gupta, G., Vij, A. and Thakur, A., 2021. Role of Fe^{3+} in altering the degrees of freedom in $ZnAl_2O_4$ spinel. Journal of Applied Physics, 130(5), p.055103. Zhang, Y., Huang, R., Li, H., Hou, D., Lin, Z., Song, J., Guo, Y., Lin, H., Song, C., Lin, Z. and Robertson, J., 2018. Germanium substitution Cr^{3+} doped zinc aluminate phosphors with bright and super-long near-infrared persistent luminescence. Acta Materialia, 155, pp.214-221.
13. Zhang, Y., Huang, R., Li, H., Hou, D., Lin, Z., Song, J., Guo, Y., Lin, H., Song, C., Lin, Z. and Robertson, J., 2018. Germanium substitution Cr^{3+} doped zinc aluminate phosphors with bright and super-long near-infrared persistent luminescence. Acta Materialia, 155, pp.214-221.
14. Siragam, S., Dubey, R.S., Pappula, L. and Babu, G.S., 2022. Zinc Aluminate-Based Composite Nanoparticles for Microwave Applications. ACS omega, 7(27), pp.23393-23400.
15. Neves, M.C., Trindade, T., Peres, M., Wang, J., Soares, M.J., Neves, A. and Monteiro, T., 2005. Photoluminescence of zinc oxide supported on submicron silica particles. Materials Science and Engineering: C, 25(5-8), pp.654-657.
16. Motloung, S.V., Dejene, F.B., Swart, H.C. and Ntwaeaborwa, O.M., 2014. Effects of Pb^{2+} ions concentration on the structure and PL intensity of Pb -doped $ZnAl_2O_4$nanocrystals synthesized using sol–gel process. Journal of sol-gel science and technology, 70(3), pp.422-427.
17. Jain, M., Kumar, M., Lee, H.H., Won, S.O., Chae, K.H., Gupta, G., Vij, A. and Thakur, A., 2021. Thermally induced cation ordering in $ZnAl_2O_4$:Mg^{2+}, Fe^{3+} for sensing thermal history through photoluminescence. Journal of Materials Science, 56(21), pp.12111-12120.
18. Eryong, N., Donglai, L., Yunsen, Z., Xue, B., Liang, Y., Yong, J., Zhifeng, J. and Xiaosong, S., 2011. Photoluminescence and magnetic properties of Fe-doped ZnS nano-particles synthesized by chemical co-precipitation. Applied surface science, 257(21), pp.8762-8766.
19. Kumar, K., Chitkara, M., Sandhu, I.S., Mehta, D. and Kumar, S., 2014. Photocatalytic, optical and magnetic properties of Fe-doped ZnO nanoparticles prepared by chemical route. Journal of Alloys and Compounds, 588, pp.681-689.
20. Wen-Chen, Z., Xiao-Xuan, W., Lv, H. and Yang, M., 2007. An alternative interpretation of the optical spectra for Fe^{3+}-doped $KTaO_3$ crystals. Journal of luminescence, 126(1), pp.91-93.
21. Pott, G.T. and McNicol, B.D., 1973. The luminescence of Fe^{3+} and Cr^{3+} in α-gallia. Journal of Luminescence, 6(3), pp.225-228.